nature materials

SUPPLEMENTARY INFORMATION

DOI: 10.1038/NMAT4202

Curvature-induced symmetry breaking determines elastic surface patterns

Norbert Stoop[1], Romain Lagrange[1], Denis Terwagne[2*], Pedro M. Reis[2,3], and Jörn Dunkel[1]

[1] *Department of Mathematics, Massachussetts Institute of Technology, 77 Massachusetts Avenue, Cambridge, MA 02139-4307, USA*

[2] *Department of Civil & Environmental Engineering, Massachussetts Institute of Technology, 77 Massachusetts Avenue, Cambridge, MA 02139-4307, USA*

[3] *Department of Mechanical Engineering, Massachussetts Institute of Technology, 77 Massachusetts Avenue, Cambridge, MA 02139-1713, USA*

(Dated: December 14, 2014)

We derive an effective theory for the wrinkling of thin hard films bound to arbitrarily curved soft substrates. Starting from the nonlinear Koiter shell equations, we show that the elastic equations can be reduced to a generalized Swift-Hohenberg theory, yielding Eq. (1) in the Main Text for the special case of a spherical surface geometry. Using nonlinear analysis of this effective fourth-order equation, we derive predictions for hexagonal and labyrinth-like wrinkling patterns in dependence on the film stress and the substrate curvature. To illustrate the effects of spatially varying substrate curvature on wrinkling, we present additional numerical results for a toroidal geometry.

DEFINITIONS

Let $\boldsymbol{S} = \boldsymbol{\Theta}(\theta_1, \theta_2)$ be a two-dimensional surface in $\mathbb{R}^3$, parameterized by $y = (\theta_1, \theta_2) \in \omega \subset \mathbb{R}^2$. Throughout, Greek indices $\alpha, \beta, \ldots$ take values in $\{1, 2\}$, whereas Latin indices $i, j, \ldots$ run from 1 to 3. The induced metric $a_{\alpha\beta}$ (first fundamental form) on the surface $\boldsymbol{S} = \boldsymbol{\Theta}(\theta_1, \theta_2)$ is given by

$$a_{\alpha\beta} = \boldsymbol{a}_\alpha \cdot \boldsymbol{a}_\beta = a_{\beta\alpha}, \tag{1}$$

where

$$\boldsymbol{a}_\alpha = \boldsymbol{\Theta}_{,\alpha} \equiv \partial_\alpha \boldsymbol{\Theta} \equiv \frac{\partial \boldsymbol{\Theta}}{\partial \theta_\alpha} \tag{2}$$

are the tangent vectors, and $\cdot$ denotes the Euclidean inner product on $\mathbb{R}^3$. The unit-length normal vector $\boldsymbol{n}$ is defined by

$$\boldsymbol{n} \equiv \boldsymbol{a}^3 = \frac{\boldsymbol{a}_1 \times \boldsymbol{a}_2}{|\boldsymbol{a}_1 \times \boldsymbol{a}_2|} \tag{3}$$

and characterized by the properties

$$\begin{aligned} \boldsymbol{n} \cdot \boldsymbol{n} &= 1, \qquad \boldsymbol{n} \cdot \boldsymbol{a}_\alpha = 0, \qquad \boldsymbol{n}_{,\alpha} \cdot \boldsymbol{n} = 0 \\ \boldsymbol{n}_{,\alpha} \cdot \boldsymbol{a}_\beta &= -\boldsymbol{a}_{\alpha,\beta} \cdot \boldsymbol{n}, \qquad \boldsymbol{n} \cdot \boldsymbol{n}_{,\alpha\beta} = -\boldsymbol{n}_{,\alpha} \cdot \boldsymbol{n}_{,\beta} \end{aligned}$$

The surface element is

$$d\omega = \sqrt{|\det(a_{\alpha\beta})|}\, dy \tag{4}$$

We also introduce the second and third fundamental forms $b_{\alpha\beta}$, $c_{\alpha\beta}$ with components given by

$$b_{\alpha\beta} = \boldsymbol{n} \cdot \boldsymbol{a}_{\alpha,\beta} \tag{5a}$$

$$c_{\alpha\beta} = \boldsymbol{n}_{,\alpha} \cdot \boldsymbol{n}_{,\beta} \tag{5b}$$

The second fundamental form, $b_{\alpha\beta}$, is often also referred to as the curvature tensor. The Christoffel symbols are

$$\Gamma^\sigma_{\alpha\beta} = \frac{1}{2} a^{\sigma\gamma} \left(a_{\gamma\alpha,\beta} + a_{\gamma\beta,\alpha} - a_{\alpha\beta,\delta} \right) \tag{6}$$

where $a^{\alpha\beta}$ are the components of the contravariant metric tensor, defined by $a^{\alpha\gamma} a_{\beta\gamma} = \delta^\alpha_\beta$. Introducing $\boldsymbol{a}^\alpha = a^{\alpha\beta} \boldsymbol{a}_\beta$, the following identities will be useful later:

$$\boldsymbol{n}_\alpha = -b_{\alpha\beta} \boldsymbol{a}^\beta = -b^\sigma_\alpha \boldsymbol{a}_\sigma \tag{7a}$$

$$b^\gamma_\alpha b_{\beta\gamma} = \boldsymbol{n}_{,\alpha} \cdot \boldsymbol{n}_{,\beta} = c_{\alpha\beta} \tag{7b}$$

The covariant derivative of a scalar function ψ is

$$\nabla_\alpha \psi = \psi_{,\alpha} \tag{8}$$

The gradient of ψ on the surface $\boldsymbol{S}$ has components

$$\nabla^\alpha \psi = a^{\alpha\beta} \nabla_\alpha \psi \tag{9}$$

The action of the Laplace-Beltrami operator $\triangle$ on scalar functions is defined as

$$\triangle \psi = \nabla_\alpha \nabla^\alpha \psi = a^{\gamma\delta} \psi_{,\gamma\delta} - a^{\gamma\delta} \Gamma^\lambda_{\gamma\delta} \psi_{,\lambda} \tag{10}$$

For a vector field V^α or for a $(0,1)-$tensor field V_α, the covariant derivative involves the Christoffel symbols,

$$\nabla_\alpha V^\beta = V^\beta_{,\alpha} + \Gamma^\alpha_{\beta\gamma} V^\gamma \tag{11a}$$

$$\nabla_\alpha V_\beta = V_{\beta,\alpha} - \Gamma^\gamma_{\alpha\beta} V_\gamma \tag{11b}$$

All gradients ∇ and Laplacians $\triangle$ below refer to these surface-specific differential operators.

*Current address: Faculté des Sciences, Université Libre de Bruxelles (ULB), Bruxelles 1050, Belgium

DOI: 10.1038/NMAT4202

ENERGY FUNCTIONAL

We extend the classical Koiter shell (KS) energy functional to account for film-substrate coupling and excess stresses.

Koiter shell equations

The KS equations describe the equilibrium of a thin shell (precurved plate) when the thickness h of the shell is small compared to its curvature in undeformed and deformed configurations. The KS equations follow rigorously by means of Γ-convergence from the full 3D elasticity problem in the limit $h \to 0$ [1].

In the absence of forces and boundary conditions, we assume that the shell adopts a stress-free equilibrium configuration which we call the reference configuration, parametrized by the surface map $\boldsymbol{\Theta}$, with fundamental forms $a_{\alpha\beta}, b_{\alpha\beta}$ etc. as specified above. Under the influence of forces and boundary conditions, the shell adopts a new, deformed configuration characterized by a displacement field $\boldsymbol{\Psi}$ defined with respect to the curved reference state $\boldsymbol{\Theta}$,

$$\boldsymbol{\Psi} = \Psi_1 \boldsymbol{a}^1 + \Psi_2 \boldsymbol{a}^2 + \Psi_3 \boldsymbol{a}^3 \equiv \Psi_i \boldsymbol{a}^i \tag{12}$$

For any point $y \in \omega$, its displaced position is given by $\boldsymbol{\Theta}(y) + \boldsymbol{\Psi}(y)$, and the respective surface geometry will be denoted as $a_{\alpha\beta}(\boldsymbol{\Psi}), b_{\alpha\beta}(\boldsymbol{\Psi})$ etc.

The KS energy of the shell is given by [1]

$$\mathcal{E}_{\mathrm{KS}}(\boldsymbol{\Psi}) = \mathcal{E}_b(\boldsymbol{\Psi}) + \mathcal{E}_s(\boldsymbol{\Psi}) + \mathcal{E}_f(\boldsymbol{\Psi}) \tag{13a}$$

with bending energy

$$\mathcal{E}_b = \frac{E_f}{2(1-\nu^2)} \int_\omega d\omega \, \frac{h^3}{24} C^{\alpha\beta\gamma\delta} R_{\gamma\delta}(\boldsymbol{\Psi}) R_{\alpha\beta}(\boldsymbol{\Psi}) \tag{13b}$$

stretching energy

$$\mathcal{E}_s = \frac{E_f}{2(1-\nu^2)} \int_\omega d\omega \, \frac{h}{2} C^{\alpha\beta\gamma\delta} G_{\gamma\delta}(\boldsymbol{\Psi}) G_{\alpha\beta}(\boldsymbol{\Psi}) \tag{13c}$$

and energy contributions

$$\mathcal{E}_f = -\int_\omega d\omega \, p^i \Psi_i \tag{13d}$$

due to external forces p^i (pressure, body loads, etc.). In Eqs. (13), E_f denotes the Young modulus of the film, ν its Poisson ratio and $C^{\alpha\beta\gamma\delta}$ the constitutive tensor. We focus on the case of a Kirchhoff-St. Venant material, corresponding to an extension of Hook's law to large deformations, described by

$$C^{\alpha\beta\gamma\delta} = (1-\nu)(a^{\alpha\delta}a^{\beta\gamma} + a^{\alpha\gamma}a^{\beta\delta}) + 2\nu a^{\alpha\beta}a^{\gamma\delta} \tag{14}$$

The nonlinear membrane bending and stretching strains $R_{\alpha\beta}$ and $G_{\alpha\beta}$ are given by [1]

$$R_{\alpha\beta} = b_{\alpha\beta}(\boldsymbol{\Psi}) - b_{\alpha\beta} \tag{15a}$$

$$G_{\alpha\beta} = \frac{1}{2}\left[a_{\alpha\beta}(\boldsymbol{\Psi}) - a_{\alpha\beta}\right] \tag{15b}$$

The bending energy scales with h^3 and will be small compared to the stretching contributions. We will therefore linearize $R_{\alpha\beta}(\boldsymbol{\Psi})$ in the bending energy, but keep higher-order terms in the stretching strains $G_{\alpha\beta}$.

Normal component of bending strains. The linearized bending strains read [1]

$$R_{\alpha\beta} \simeq (\boldsymbol{\Psi}_{,\alpha\beta} - \Gamma^\sigma_{\alpha\beta}\boldsymbol{\Psi}_{,\sigma}) \cdot \boldsymbol{n} \tag{16}$$

With this approximation, the normal displacement component Ψ_3 decouples from the in-plane components. Since the dominant bending contribution comes from the normal displacement Ψ_3, we may neglect the in-plane components

$$\begin{aligned} R_{\alpha\beta} \simeq \rho_{\alpha\beta}(\Psi_3) &\equiv \Psi_{3,\alpha\beta} - \Gamma^\sigma_{\alpha\beta}\Psi_{3,\sigma} - \Psi_3 c_{\alpha\beta} \\ &= \nabla_\alpha \nabla_\beta \Psi_3 - \Psi_3 c_{\alpha\beta} \end{aligned} \tag{17}$$

Normal component of stretching strains. For the stretching strains, one has [1]

$$\begin{aligned} G_{\alpha\beta} &= \frac{1}{2}\left(\nabla_\beta \Psi_\alpha + \nabla_\alpha \Psi_\beta + \boldsymbol{\Psi}_{,\alpha} \cdot \boldsymbol{\Psi}_{,\beta}\right) - b_{\alpha\beta}\Psi_3 \\ &= \frac{1}{2}(\Psi_{\alpha,\beta} + \Psi_{\beta,\alpha} + \boldsymbol{\Psi}_{,\alpha} \cdot \boldsymbol{\Psi}_{,\beta}) - \Gamma^\sigma_{\alpha\beta}\Psi_\sigma - b_{\alpha\beta}\Psi_3 \end{aligned} \tag{18}$$

The displacement derivative can be split into an in-plane and normal part,

$$\boldsymbol{\Psi}_{,\alpha} = (\Psi_{\gamma,\alpha} - \Gamma^\sigma_{\alpha\gamma}\Psi_\sigma - b_{\alpha\gamma}\Psi_3)\boldsymbol{a}^\gamma + (\Psi_{3,\alpha} + b^\gamma_\alpha \Psi_\gamma)\boldsymbol{a}^3$$

Due to the orthogonality of $\boldsymbol{a}^\alpha$ and $\boldsymbol{n} \equiv \boldsymbol{a}^3$, the nonlinear term in the stretching strains becomes

$$\boldsymbol{\Psi}_{,\alpha} \cdot \boldsymbol{\Psi}_{,\beta} = t^\delta_\alpha t_{\beta\delta} + s_\alpha s_\beta \tag{19a}$$

where

$$t_{\alpha\beta} = \Psi_{\beta,\alpha} - \Gamma^\sigma_{\alpha\beta}\Psi_\sigma - b_{\alpha\beta}\Psi_3 \tag{19b}$$

$$s_\alpha = \Psi_{3,\alpha} + b^\sigma_\alpha \Psi_\sigma \tag{19c}$$

Expanding Eqs. (19) for small in-plane displacements, $|\Psi_\alpha| \ll |\Psi_3|$, one finds to leading order

$$\boldsymbol{\Psi}_{,\alpha} \cdot \boldsymbol{\Psi}_{,\beta} \simeq \Psi_{3,\alpha}\Psi_{3,\beta} + b^\delta_\alpha b_{\beta\delta}(\Psi_3)^2$$

Using Eq. (7) and (18), we obtain

$$G_{\alpha\beta} \simeq \gamma_{\alpha\beta}(\Psi_3) \equiv \frac{1}{2}[\Psi_{3,\alpha}\Psi_{3,\beta} + c_{\alpha\beta}(\Psi_3)^2] - b_{\alpha\beta}\Psi_3 \tag{20}$$

We note that the obtained bending and stretching strains are symmetric,

$$\rho_{\alpha\beta} = \rho_{\beta\alpha}, \qquad \gamma_{\alpha\beta} = \gamma_{\beta\alpha} \tag{21}$$

Additional remarks. In our and previous [2] experiments, the film stress is imposed in two ways: (i) depressurization of the shell-substrate system and (ii) swelling of the film. Before the onset of the buckling transition, either technique creates a pre-stress in the film. The associated prestrain can be decomposed into an in-plane part $\bar{\gamma}_{\alpha\beta}$ and a bending part $\bar{\rho}_{\alpha\beta}$, with $\bar{\gamma}_{\alpha\beta} \gg \bar{\rho}_{\alpha\beta}$. Adopting the same approximations as above (Eqs. 17, 20), the prestrains remain symmetric. Restricting ourselves furthermore to equi-biaxial pre-stress without shear, $\bar{\gamma}_{\alpha\beta}$ is proportional to the metric tensor $a_{\alpha\beta}$, and we write this as

$$\bar{\gamma}_{\alpha\beta} = \bar{\gamma}\, a_{\alpha\beta} \tag{22}$$

where from now on $\bar{\gamma}$ denotes the constant of proportionality.

If the film stress due to depressurization or swelling becomes too large, the film will buckle, with an inhomogeneous deformation u around the pre-stressed state. The strains of a buckled configuration can then be expressed as

$$\gamma_{\alpha\beta}(u_0+u) = \bar{\gamma}_{\alpha\beta} + \frac{1}{2}\left(u_{,\alpha}u_{,\beta} - 2b_{\alpha\beta}u + c_{\alpha\beta}u^2\right) \tag{23a}$$

$$\rho_{\alpha\beta}(u_0+u) = \bar{\rho}_{\alpha\beta} + \nabla_\alpha\nabla_\beta u - c_{\alpha\beta}u \tag{23b}$$

To contract the strains with the constitutive tensor, we use the fact that the bending and stretching strains, Eqs. (23), are symmetric. For any symmetric $(0,2)$-tensor $\tau_{\alpha\beta}$, the contraction $\mathcal{C}(\tau)$ of $C^{\alpha\beta\gamma\delta}$ with $\tau_{\alpha\beta}$ can be written as

$$\begin{aligned}\mathcal{C}(\tau) &= C^{\alpha\beta\gamma\delta}\tau_{\alpha\beta}\tau_{\gamma\delta}\\ &= 2\left[(1-\nu)\tau^{\alpha\beta}\tau_{\alpha\beta} + \nu(\tau^\gamma_\gamma)^2\right]\\ &= 2\left(\tau_M + \tau_G\right)\end{aligned} \tag{24}$$

with

$$\begin{aligned}\tau_M &= (\tau^\gamma_\gamma)^2\\ \tau_G &= (1-\nu)\left[\tau^{\alpha\beta}\tau_{\alpha\beta} - (\tau^\gamma_\gamma)^2\right]\end{aligned} \tag{25}$$

For later use, it is convenient to introduce the identities

$$\mathcal{H} = \frac{1}{2}b^\gamma_\gamma \tag{26a}$$

$$\mathcal{K} = \det(\{a_{\alpha\beta}\})/\det(\{b_{\alpha\beta}\}) \tag{26b}$$

$$\mathcal{R} \equiv b^{\alpha\beta}b_{\alpha\beta} = c^\gamma_\gamma = 4\mathcal{H}^2 - 2\mathcal{K} \tag{26c}$$

$$\mathcal{S} \equiv b^{\alpha\beta}c_{\alpha\beta} = 2\mathcal{H}(4\mathcal{H}^2 - 3\mathcal{K}) \tag{26d}$$

$$\mathcal{T} \equiv c^{\alpha\beta}c_{\alpha\beta} = 16\mathcal{H}^2(\mathcal{H}^2 - \mathcal{K}) + 2\mathcal{K}^2 \tag{26e}$$

$\mathcal{H}$ is the mean curvature and $\mathcal{K}$ the Gaussian curvature. Most of these expressions follow directly from the contracted Gauss-Codazzi-Mainardi equations [3].

Relevant energy contributions

Bending energy density. Using the definition of the Laplace-Beltrami operator, Eq. (10), and Eq. (24) with $\tau_{\alpha\beta} = \rho_{\alpha\beta}$, the mean-curvature contribution ρ_M can be written as

$$\begin{aligned}\rho_M = \left(\rho^\gamma_\gamma\right)^2 = (\triangle u)^2 - 2\mathcal{R}u\triangle u + \mathcal{R}^2u^2 +\\ 2(\bar{\rho}^\gamma_\gamma\triangle u - \mathcal{R}\bar{\rho}^\gamma_\gamma u) + (\bar{\rho}^\gamma_\gamma)^2\end{aligned} \tag{27}$$

The ρ_G-term in Eq. (24) accounts for the energy cost due to a change of Gaussian curvature. This term is negligible if the typical wrinkling wavelengths are small compared to the local radii of curvature of the underlying surface. More precisely, in this case, one finds that Eqs. (15a,17) reduce to $\rho^\beta_\alpha \simeq b^\beta_\alpha(u)$ in leading order, where $b^\beta_\alpha(u)$ is the curvature tensor of the deformed configuration. Accordingly, Eq. (25) then yields $\rho_G = (1-\nu)\mathcal{K}(u)$. Since the Gaussian curvature $\mathcal{K}(u)$ of the deformed configuration integrates to a topological invariant for a closed surface (or when the geodesic curvature of the boundary curve is fixed), the ρ_G-term can be neglected in the variational formulation, just as in the classical Helfrich model [4]. Under these assumptions, the resulting bending energy takes the form

$$\begin{aligned}\mathcal{E}_b = \frac{E_f}{2(1-\nu^2)}\int_\omega d\omega\,\frac{h^3}{12}\left[(\triangle u)^2 + 2\mathcal{R}(\nabla u)^2 +\right.\\ (\mathcal{R}^2 - \triangle\mathcal{R})u^2 +\\ \left. 2\left(\triangle\bar{\rho}^\gamma_\gamma - \mathcal{R}\bar{\rho}^\gamma_\gamma\right)u + (\bar{\rho}^\gamma_\gamma)^2\right]\end{aligned} \tag{28}$$

where from now on the product symbol $\cdot$ as in $(\nabla u)^2 = (\nabla u)\cdot(\nabla u)$ denotes the scalar product with respect to the surface metric. To obtain Eq. (28), we used the generalized Stokes theorem[1] to rewrite the second and fourth term on the rhs. of Eq. (27).

Stretching energy density. For the stretching energy

$$\mathcal{E}_s = \frac{E_f}{2(1-\nu^2)}\int_\omega d\omega\,\frac{h}{2}\mathcal{C}(\gamma) \tag{29}$$

we find by using Eq. (24) with $\tau_{\alpha\beta} = \gamma_{\alpha\beta}$, and combining with Eqs. (22), (23) and (26),

$$\begin{aligned}\mathcal{C}(\gamma) = 2(1+\nu)\bar{\gamma}(\nabla u)^2 + 2(1+\nu)(\nabla u)^4 -\\ 2\left[(1-\nu)b^{\alpha\beta}\nabla_\alpha u\nabla_\beta u + 2\nu\mathcal{H}(\nabla u)^2\right]u +\\ \left[(1-\nu)c^{\alpha\beta}\nabla_\alpha u\nabla_\beta u + \nu\mathcal{R}(\nabla u)^2\right]u^2 +\\ 2\left[(1-\nu+\bar{\gamma}+\nu\bar{\gamma})\mathcal{R} + 4\nu\mathcal{H}^2\right]u^2 -\\ 2\left[(1-\nu)\mathcal{S} + 2\nu\mathcal{H}\mathcal{R}\right]u^3 +\\ \tfrac{1}{2}\left[(1-\nu)\mathcal{T} + \nu\mathcal{R}^2\right]u^4 + \mathcal{O}(1) + \mathcal{O}(u)\end{aligned} \tag{30}$$

[1] Note that $-\int d\omega\,\mathcal{R}u\triangle u = \int d\omega\,u(\nabla\mathcal{R})\cdot(\nabla u) + \int d\omega\,\mathcal{R}(\nabla u)^2$. Furthermore, repeated application of the Stokes theorem gives $\int d\omega\,u(\nabla\mathcal{R})\cdot(\nabla u) = \frac{1}{2}\int d\omega\,\triangle\mathcal{R}u^2$.

DOI: 10.1038/NMAT4202

where we did not explicitly write down the terms linear and constant in u, as they will not be relevant for the later analysis (see detailed remarks in *Total energy density* below).

Substrate coupling energy. In our experiments, the thin film is coupled to a curved soft substrate. To simplify further analysis, we assume from now on that the substrate has the same Poisson ratio ν as the film, as is the case in our experiments. We model the substrate coupling as a nonlinear spring by adding a substrate energy $\mathcal{E}_{sub}$ to the KS energy from Eq. (13a), where

$$\mathcal{E}_{sub} = \frac{E_s}{2}\int_\omega d\omega \left(Au + \frac{\tilde{a}}{h}u^2 + \frac{\tilde{c}}{h^3}u^4\right) \tag{31}$$

with E_s denoting the Young modulus of the substrate. The constant film thickness h could have been absorbed into the coefficients $\tilde{a}$ and $\tilde{c}$, but simplifies subsequent formulas. Note that $\mathcal{E}_{sub}$ contains a term linear in u because we are considering the state of the film-substrate system around a flat but displaced equilibrium solution u_0. This linear term gives rise to a corresponding constant normal force that is needed to balance the internal normal forces of the film.

Energy due to excess film stress. Finally, we still have to account for the excess film stress

$$\Sigma_e \equiv \frac{\sigma}{\sigma_c} - 1 \tag{32a}$$

where σ is the film stress and σ_c the critical stress needed for wrinkling. In our model, the energy due to excess film stress is included by adding a term

$$\mathcal{E}_\sigma = \frac{E_f}{2(1-\nu^2)}\int_\omega d\omega\, \frac{\tilde{a}_2}{h}\Sigma_e u^2 \tag{32b}$$

to the KS energy from Eq. (13a). The energy contribution $\mathcal{E}_\sigma$ is crucial for capturing the system behavior beyond the wrinkling instability. We discuss below how the dimensionless parameter $\tilde{a}_2$ is related to the elastic properties of the substrate. The u^2-dependence of $\mathcal{E}_\sigma$ is a classical result from elastic wrinkling theory [5], ensuring that the amplitude-stress relationship in the effective model agrees with classical wrinkling theory, as is shown in detail further below.

Total energy density. Adding the contributions due to substrate coupling, external forces and excess stress to the KS energy (13a), we obtain the total elastic energy

$$\mathcal{E} = \frac{E_f}{1-\nu^2}\bar{\mathcal{E}} \tag{33a}$$

where to leading order

$$\begin{aligned}\bar{\mathcal{E}} = \int_\omega d\omega \Big[&\frac{\gamma_0}{2}(\nabla u)^2 + \frac{\gamma_2}{2}(\triangle u)^2 + \frac{a}{2}u^2 + \frac{b}{3}u^3 + \frac{c}{4}u^4 - \\ &\frac{h}{2}\left[(1-\nu)b^{\alpha\beta}\nabla_\alpha u\nabla_\beta u + 2\nu\mathcal{H}(\nabla u)^2\right]u + \\ &\frac{h}{4}\left[(1-\nu)c^{\alpha\beta}\nabla_\alpha u\nabla_\beta u + \nu\mathcal{R}(\nabla u)^2\right]u^2\Big]\end{aligned} \tag{33b}$$

with coefficients

$$\begin{aligned}\gamma_0 &= h\bar{\gamma}(1+\nu) + \frac{h^3\mathcal{R}}{6} \\ \gamma_2 &= \frac{h^3}{12} \\ a &= h\left[(1-\nu+\bar{\gamma}+\nu\bar{\gamma})\mathcal{R} + 4\nu\mathcal{H}^2\right] + \frac{h^3(\mathcal{R}^2-\triangle\mathcal{R})}{12} + \\ &\quad \frac{E_s(1-\nu^2)}{E_f}\frac{\tilde{a}}{h} + \frac{\tilde{a}_2}{h}\Sigma_e \\ b &= -\frac{3h}{2}\left[(1-\nu)\mathcal{S} + 2\nu\mathcal{H}\mathcal{R}\right] \\ c &= \frac{h}{2}\left[(1-\nu)\mathcal{T} + \nu\mathcal{R}^2\right] + 2\frac{E_s(1-\nu^2)}{E_f}\tilde{c}\end{aligned} \tag{33c}$$

Note that for compressive stresses $\bar{\gamma} < 0$. Thus, for sufficiently large film pre-stress, $\gamma_0 < 0$. To obtain the effective energy functional (33), the following additional simplifications and assumptions were adopted:

- **Constant terms.** We neglected all constant terms in the energy, as they will not contribute to the equations of motion, obtained by variation of the energy with respect to u.
- **Terms linear in u.** We note that the term linear in u gives rise to a inhomogeneous, constant term in the equation of motion. However, $u = 0$ always is an equilibrium solution by construction. More precisely, $u = 0$ means that the film is radially displaced by u_0, which is a fundamental solution of the problem. Therefore, the inhomogeneous term in the equation of motion has to vanish, implying that the coefficient of the energy term linear in u must be zero. This condition can be interpreted as follows: For $u = 0$ to be an equilibrium solution, the sum of all normal forces acting on the film must vanish.
- **Quartic terms.** The quartic terms in u and ∇u ensure that the effective theory remains stable above the wrinkling threshold, as these terms limit the growth of the most unstable modes. To keep the theory as simple as possible, we only include the dominant u^4-contribution and neglect terms $\propto (\nabla u)^4$.

Taking the variation of $\bar{\mathcal{E}}$ with respect to u, we obtain

$$\begin{aligned}-\frac{\delta\bar{\mathcal{E}}}{\delta u} = {}&\gamma_0\triangle u - \gamma_2\triangle^2 u - au - bu^2 - cu^3 + \\ &\frac{h}{2}\left\{(\nu-1)\left[b^{\alpha\beta}\nabla_\alpha u\nabla_\beta u + 2u\nabla_\beta\left(b^{\alpha\beta}\nabla_\alpha u\right)\right] + \right. \\ &\left. 2\nu\left[\mathcal{H}(\nabla u)^2 - 2\nabla\cdot(\mathcal{H}u\nabla u)\right]\right\} + \\ &\frac{h}{2}\left[(1-\nu)u\nabla_\beta\left(uc^{\alpha\beta}\nabla_\alpha u\right) - \nu\mathcal{R}u(\nabla u)^2 + \right. \\ &\left.\nu\nabla\cdot(\mathcal{R}u^2\nabla u)\right]\end{aligned} \tag{34}$$

where $\nabla\cdot$ denotes the surface divergence. We note that, for a flat Euclidean metric, the first line of Eq. (34) coincides with the Swift-Hohenberg (SH) equation, as originally derived in the context of Rayleigh-Bénard convection [6, 7]. The b-term and the first term $\propto h$ (second and third line) break the symmetry $u \to -u$, which is known to lead to a transition from labyrinth-like patterns to hexagons for SH-like equations. As both terms depend on the curvature tensor $b_{\alpha\beta}$, we can infer that regions of high curvature will show different wrinkling patterns than regions of low curvature.

We next apply Eq. (34) to derive quantitative predictions for wrinkling patterns transitions on spherical geometries, which are then compared with our experiments (Main Text). Subsequently, we still present numerical solutions for a toroidal geometry, as an example of a surface with locally varying curvature.

APPLICATION TO SPHERICAL GEOMETRIES

Using spherical coordinates $(\theta_1, \theta_2) \in [0, 2\pi) \times [0, \pi]$, a spherical surface of radius R is described by the metric tensor

$$(a_{\alpha\beta}) = \begin{pmatrix} (R\sin\theta_2)^2 & 0 \\ 0 & R^2 \end{pmatrix} \tag{35}$$

In this case, we have $\mathcal{H} = -1/R$, $\mathcal{K} = 1/R^2$. Thus

$$\mathcal{R} = 2/R^2, \qquad \mathcal{S} = -2/R^3, \qquad \mathcal{T} = 2/R^4 \tag{36}$$

Total energy density. Noting that the sphere has constant mean and Gaussian curvature $\mathcal{H}$ and $\mathcal{K}$, Eq. (36) allows to simplify the total energy density (33) considerably,

$$\bar{\mathcal{E}} = \int_\omega d\omega \left[\frac{\gamma_0}{2} (\nabla u)^2 + \frac{\gamma_2}{2} (\triangle u)^2 + \frac{a}{2}u^2 + \frac{b}{3}u^3 + \frac{c}{4}u^4 + \Gamma_1 (\nabla u)^2 u + \frac{\Gamma_2}{2} (\nabla u)^2 u^2 \right] \tag{37}$$

with coefficients

$$\begin{aligned} \gamma_0 &= h\bar{\gamma}(1+\nu) + \frac{h^3}{3R^2} \\ \gamma_2 &= \frac{h^3}{12} \\ a &= \frac{2h(1+\bar{\gamma})(1+\nu)}{R^2} + \frac{h^3}{3R^4} + \frac{E_s(1-\nu^2)}{E_f}\frac{\tilde{a}}{h} + \frac{\tilde{a}_2}{h}\Sigma_e \\ b &= \frac{3h(1+\nu)}{R^3} \\ c &= \frac{h(1+\nu)}{R^4} + 2\frac{E_s(1-\nu^2)}{E_f}\tilde{c} \\ \Gamma_1 &= \frac{h(1+\nu)}{2R} \\ \Gamma_2 &= \frac{h(1+\nu)}{2R^2} \end{aligned} \tag{38}$$

Equations of motions

To identify the equilibrium configurations, we assume that the film exhibits an overdamped relaxation dynamics. Then, the equations of motion follow by functional variation of the elastic energy (37) with respect to the displacement field u,

$$\frac{\rho}{\tau_0}\partial_t u = -\frac{\delta\mathcal{E}}{\delta u} \tag{39}$$

where ρ is the constant surface mass density of the film and τ_0 the damping-time scale. The relaxation dynamics (39) can be written in the equivalent form

$$\mu\partial_t u = -\frac{\delta\bar{\mathcal{E}}}{\delta u} \tag{40a}$$

where the coefficient

$$\mu = \frac{\rho(1-\nu^2)}{\tau_0 E_f} \tag{40b}$$

is the inverse relaxation speed. Calculating the functional derivative $\delta\bar{\mathcal{E}}/\delta u$ gives

$$\begin{aligned} \mu\partial_t u \;=\; & \gamma_0\triangle u - \gamma_2\triangle^2 u - au - bu^2 - cu^3 + \\ & \Gamma_1\left[(\nabla u)^2 + 2u\triangle u\right] + \Gamma_2\left[u(\nabla u)^2 + u^2\triangle u\right] \end{aligned} \tag{41}$$

Since we are only interested in the steady-state solutions, the exact value of μ is not relevant for our analysis. It is convenient to rewrite Eq. (41) in dimensionless form by measuring length in units of the film thickness h and time in units of $\tau_h = \mu h$. Introducing the dimensionless curvature parameter

$$\kappa = h/R \tag{42}$$

Eq. (41) reduces to

$$\begin{aligned} \partial_t u \;=\; & \gamma_0\triangle u - \gamma_2\triangle^2 u - au - bu^2 - cu^3 + \\ & \Gamma_1\left[(\nabla u)^2 + 2u\triangle u\right] + \Gamma_2\left[u(\nabla u)^2 + u^2\triangle u\right] \end{aligned} \tag{43}$$

with rescaled dimensionless parameters

$$\begin{aligned} \gamma_0 &= \bar{\gamma}(1+\nu) + \frac{\kappa^2}{3} < 0 \\ \gamma_2 &= \frac{1}{12} \\ a &= 2(1+\bar{\gamma})(1+\nu)\kappa^2 + \frac{\kappa^4}{3} + \frac{E_s(1-\nu^2)}{E_f}\tilde{a} + \tilde{a}_2\Sigma_e \\ b &= 3(1+\nu)\kappa^3 \\ c &= (1+\nu)\kappa^4 + 2\frac{E_s(1-\nu^2)}{E_f}\tilde{c} \\ \Gamma_1 &= \frac{(1+\nu)\kappa}{2} \\ \Gamma_2 &= \frac{(1+\nu)\kappa^2}{2} \end{aligned} \tag{44}$$

DOI: 10.1038/NMAT4202

Note that the covariant derivatives ∇ and $\triangle$ in Eq. (43) are now also defined with respect to the rescaled dimensionless sphere of radius $\kappa^{-1} = R/h$. In Eq. (44), we kept the term $\sim \kappa^4$ in the coefficient a. Although this higher order term is negligible, its inclusion will lead to simpler expressions when matching our model with experiments (see section *Curvature-dependence of the critical strain* $\bar{\gamma}$ below). Given the dimensionless parameters in Eq. (44), the corresponding values in physical units are recovered through the transformations

$$\begin{aligned} u &\to hu, & R &\to h/\kappa, & t &\to \mu h t \\ \gamma_0 &\to h\gamma_0, & \gamma_2 &\to h^3\gamma_2 & & \\ a &\to a/h, & b &\to b/h^2, & c &\to c/h^3 \\ \Gamma_1 &\to \Gamma_1, & \Gamma_2 &\to \Gamma_2/h & & \end{aligned} \tag{45}$$

As evident from Eq. (44), the model is specified through dimensionless parameters

$$(\kappa, \bar{\gamma}, E_s/E_f, \nu, \tilde{a}, \tilde{a}_2, \tilde{c}) \tag{46}$$

Parameter determination

The parameters (h, R, ν, E_s, E_f) can be directly measured for our experimental system. To determine the remaining parameters $(\bar{\gamma}, \tilde{a}, \tilde{a}_2, \tilde{c})$, we proceed as follows:

1. Linear stability analysis will enable us to relate γ_0 at the onset of wrinkling with the wavelength λ, which yields a relation between the critical buckling strain $\bar{\gamma}$ and the ratio E_s/E_f.

2. The value of the substrate parameter $\tilde{a}$ can be estimated from known results for the critical bulking stress in planar elasticity theory [8]. Below, we will extend the classical derivation to the weakly curved case to confirm that our model predictions agree with recent results by Cai *et al.* [9]

3. By means of nonlinear stability analysis and comparison with analytical results for the standard Swift-Hohenberg equation, we will express the parameter $\tilde{a}_2$ in terms of c, leaving $\tilde{c}$ as the only remaining fit parameter. We estimate $\tilde{c}$ by comparing our numerical simulations with the experimentally measured surface morphologies.

Critical stress $\bar{\gamma}$ and $\tilde{a}$

We estimate $\bar{\gamma}$ by comparing our effective theory with known results for the full elastic equations in the planar limit case $R \to \infty$. Letting $\kappa \to 0$ and linearizing Eq. (43) for a small perturbation εe^{ikx} of the unbuckled homogeneous solution, one finds the dominant unstable wave-mode

$$|k| = \sqrt{\frac{|\gamma_0|}{2\gamma_2}} = \sqrt{6|\gamma_0|} \tag{47a}$$

which selects the characteristic wavelength

$$\lambda_c = \frac{2\pi}{|k|} = \frac{2\pi}{\sqrt{6|\gamma_0|}} \tag{47b}$$

Equating λ_c with the known wrinkling wavelength λ_{el} of a planar elastic film-substrate system, which in units $h = 1$ is given by [8]

$$\lambda_{el} = 2\pi \left(\frac{E_f}{3E_s}\right)^{1/3} \tag{48}$$

we obtain

$$\gamma_0 = -\frac{1}{6}\left(\frac{3E_s}{E_f}\right)^{2/3} \tag{49}$$

The sign indicates a compressive strain, which in our terminology is negative. From Eq. (44) with $\kappa \to 0$, we find the planar estimate

$$\bar{\gamma} \simeq -\frac{1}{6(1+\nu)}\left(\frac{3E_s}{E_f}\right)^{2/3} \equiv \bar{\gamma}_p \tag{50}$$

A correction due to curvature will be discussed below.

Critical stress. The strain $\bar{\gamma}_p$ can be associated with the critical stress σ_c at the wrinkling threshold. As expressed by Eq. (22), our system is in a state of equibiaxial strains $\bar{\gamma}$ implying that, in a locally orthogonal coordinate frame, the in-plane elasticity tensor reduces to $\epsilon_{11} = \epsilon_{22} = \epsilon$, $\epsilon_{12} = \epsilon_{21} = 0$. The usual stress-strain relationship of a Hookean material then reads [10]

$$\begin{aligned} \sigma_{11} = \sigma_{22} &= \frac{E}{1-\nu^2}(\epsilon_{11} + \nu\epsilon_{22}) = \frac{E}{1-\nu}\epsilon \equiv \sigma \\ \sigma_{12} = \sigma_{21} &= 0 \end{aligned}$$

Assuming a standard linear relation between stress and strain, we expect

$$\sigma_c = k_\sigma \frac{E_f}{1-\nu}\bar{\gamma}_p \tag{51}$$

with some constant prefactor k_σ. Inserting Eq. (50), we obtain

$$\sigma_c = -\frac{k_\sigma}{6}\frac{E_f}{1-\nu^2}\left(\frac{3E_s}{E_f}\right)^{2/3} \tag{52}$$

which for $k_\sigma = 3/2$ agrees with the known critical stress of elastic wrinkling analysis [8]

$$\sigma_{c_{el}} = -\frac{E_f}{4(1-\nu^2)}\left(\frac{3E_s}{E_f}\right)^{2/3} \tag{53}$$

Estimation of $\tilde{a}$ near the critical value σ_c. In the planar limit $\kappa \to 0$, Eq. (43) exhibits a bifurcation from a uniform state to nontrivial pattern formation only if $a < a_c$, where

$$a_c = \frac{\gamma_0^2}{4\gamma_2} = \frac{1}{12}\left(\frac{3E_s}{E_f}\right)^{4/3} \tag{54}$$

At the wrinkling onset, corresponding to $a = a_c$, the film stress σ equals the critical stress σ_c so that $\Sigma_e = 0$. For the planar case, Eq. (54) thus determines the substrate parameter $\tilde{a}$ as

$$\tilde{a} = \frac{1}{4(1-\nu^2)}\left(\frac{3E_s}{E_f}\right)^{1/3} \tag{55}$$

Curvature-dependence of the critical strain $\bar{\gamma}$

Recent simulations of the full coupled elasticity equations [11] and experiments with polymer colloids [12] report wave-length reduction of pattern on curved substrates compared with the planar case. It is therefore interesting to study how the critical strain $\bar{\gamma} < 0$ depends on the curvature parameter $\kappa = h/R$ in our model.

Similar to the planar case, cf. Eq. (54), the wrinkling bifurcation occurs when

$$\frac{\gamma_0^2(\kappa)}{4\gamma_2\, a_c(\kappa)} = 1. \tag{56}$$

Recalling that $\Sigma_e = 0$ at the transition point and using the the above result for $\tilde{a}$, we can solve Eq. (56) for the critical strain $\bar{\gamma}$. Using Eq. (44) we then obtain for γ_0

$$\gamma_0 = \frac{\kappa^2}{3} - \frac{1}{6}\sqrt{\left(\frac{3E_s}{E_f}\right)^{4/3} + 24(1+\nu)\kappa^2} \tag{57}$$

which reduces to Eq. (49) in the planar case ($\kappa = 0$). For $\bar{\gamma}$, we find to $\mathcal{O}(\kappa^4)$

$$\frac{\bar{\gamma}}{\bar{\gamma}_p} = 1 + 12\kappa^2(1+\nu)\left(\frac{E_f}{3E_s}\right)^{4/3} \tag{58}$$

where $\bar{\gamma}_p$ is the critical buckling strain for the planar case, given in Eq. (50). This asymptotic scaling behavior in κ is similar to the results of Cai *et al.* [9], although the numerical prefactors and the dependence on the Poisson ratio ν differ.

According to Eq. (57), the absolute value $|\gamma_0|$ increases with curvature with a leading order correction $\sim \kappa^2$. Equation (47b) then implies that the wavelength λ_c decreases with increasing curvature, in qualitative agreement with experimental and numerical findings [11, 12]. It is interesting to note that the wavelength reduction in our model is due to the nonlinear, curvature-dependent stretching terms of the underlying KS energy, unlike the model of Yin *et al.* [13], where a wavelength reduction was obtained by assuming a curvature-dependent substrate model. Unfortunately, for the range of parameters realized in our experiments the curvature-induced wavelength reduction is below the detection threshold. We therefore did not include any curvature-dependent substrate response in our model.

γ_0	=	$-\frac{\eta^{2/3}}{6} - \left[\frac{2(1+\nu)}{\eta^{2/3}} - \frac{1}{3}\right]\kappa^2$
a	=	$\frac{\eta^{4/3}}{12} + \frac{6(1+\nu)-\eta^{2/3}}{3}\kappa^2 + \tilde{a}_2\Sigma_e$
b	=	$3(1+\nu)\kappa^3$
c	=	$\frac{2(1+\nu)\eta^{2/3}}{3}c_1$
Γ_1	=	$\frac{1+\nu}{2}\kappa$
Γ_2	=	$\frac{1+\nu}{2}\kappa^2$
$\tilde{a}_2$	=	$-\frac{\eta^{4/3}(c+3\lvert\gamma_0\rvert\Gamma_2)}{48\gamma_0^2}$

TABLE I: List of parameters for Eqs. (43) and (64) as obtained by systematic asymptotic matching to classical elastic wrinkling theory, with $\eta = 3E_s/E_f$, $\gamma_2 = 1/12$, $\Sigma_e = (\sigma/\sigma_c) - 1$, and $\kappa = h/R$ where h is the film thickness and R the radius (see Fig. 2 of Main Text). We substituted $\tilde{a}$ and $\tilde{c}$ by Eqs. (55) and (77). Focusing on the leading order contribution, we only kept terms up to $\mathcal{O}(\kappa^3)$, cf. Eq. (57). The only remaining fitting parameter of the model is c_1.

Nonlinear behavior above onset

Having determined estimates for the parameters $(\bar{\gamma}, \tilde{a})$ by analyzing the onset of wrinkling, the two remaining unknown parameters are $(\tilde{a}_2, \tilde{c})$. Aiming to further reduce the number of free parameters, we now turn to the regime beyond the wrinkling threshold, where patterns are selected by nonlinear effects. To this end, we first reduce the generalized Swift-Hohenbergy equation (43) to a standard Swift-Hohenberg (SH) equation by approximating mixed $\Gamma_{1,2}$-terms in Eq. (43) that contain both u and ∇u through effective expressions that only contain u. Assuming a typical relation between pattern amplitude and excess film stress $\Sigma_e = (\sigma/\sigma_c) - 1$, we can then exploit existing results for the stability of patterns in the SH equation to predict the morphological phase diagram of the wrinkling patterns in our experimental system.

Swift-Hohenberg approximation. To approximate Eq. (43) by a standard SH equation, we recall that γ_0 and γ_2 select the dominant (most unstable) wave number vector $k_c = \pm\sqrt{6|\gamma_0|}$, see Eq. (47a). Considering the

DOI: 10.1038/NMAT4202

limit $\kappa \to 0$ and a plane-wave solution of the form

$$u = \mathcal{A}\cos(k_c x) \tag{59}$$

the Γ_1-term in Eq. (43) exerts an average force per wavelength $\lambda = 2\pi/|k_c|$ of

$$\left\langle \Gamma_1 \left[(\nabla u)^2 + 2u\triangle u \right] \right\rangle_\lambda = -\frac{1}{2}\Gamma_1 \mathcal{A}^2 k_c^2 \tag{60}$$

where

$$\langle f(x)\rangle_\lambda \equiv \frac{1}{\lambda}\int_0^\lambda dx\ f(x) \tag{61}$$

Comparing Eq. (60) with the average force exerted by a quadratic force $f = au^2$ for the wave solution (59),

$$\langle au^2\rangle_\lambda = \frac{a\mathcal{A}^2}{2} \tag{62}$$

we can approximate the Γ_1-term by an 'equivalent' average force term of the form

$$\Gamma_1 \left[(\nabla u)^2 + 2u\triangle u \right] \approx -\Gamma_1 k_c^2 u^2 \tag{63a}$$

Similarly, the average force due to the Γ_2-term can be approximated by a cubic force. Since the Γ_2-term is antisymmetric in u, the corresponding mean force is obtained by averaging over the interval $[\lambda/4, 3\lambda/4]$, yielding

$$\Gamma_2 \left[u\,(\nabla u)^2 + u^2\triangle u \right] \approx -\frac{1}{2}\Gamma_2 k_c^2 u^3 \tag{63b}$$

With these approximations, Eq. (43) reduces to the SH equation

$$\partial_t u = \gamma_0\triangle u - \gamma_2\triangle^2 u - au - \left(b + \Gamma_1 k_c^2\right) u^2 - \left(c + \frac{\Gamma_2 k_c^2}{2}\right) u^3 \tag{64}$$

To facilitate direct comparison with results in the literature [14], it is convenient to rewrite Eq. (64) in the rescaled *normal form*

$$\partial_T \phi = -2\triangle_X \phi - \triangle_X^2 \phi - A\phi - B\phi^2 - \phi^3 \tag{65}$$

where

$$\begin{aligned} T &= \frac{4\gamma_2 t}{\gamma_0^2} = \frac{t}{3\gamma_0^2} \\ \triangle_X &= \frac{\triangle}{k_c^2} = \frac{\triangle}{6|\gamma_0|} \\ \phi &= \frac{u}{u_*} \\ u_* &= \sqrt{\frac{\gamma_0^2}{4\gamma_2(c + \Gamma_2 k_c^2/2)}} = \sqrt{\frac{\gamma_0^2}{(c/3) + \Gamma_2|\gamma_0|}} \\ A &= \frac{a}{a_c} = \frac{4a\gamma_2}{\gamma_0^2} = \frac{3a}{\gamma_0^2} \\ B &= \frac{2\left(b + \Gamma_1 k_c^2\right)}{\sqrt{(\gamma_0^2/\gamma_2)\,(c + \Gamma_2 k_c^2/2)}} = u_* \frac{(b/3) + 2|\gamma_0|\Gamma_1}{\gamma_0^2} \end{aligned} \tag{66}$$

with a_c given by Eq. (54).

Excess film stress. Our model accounts for the excess film stress $\Sigma_e = (\sigma/\sigma_c) - 1$ through the contribution $\tilde{a}_2\Sigma_e$ that appears in the coefficient a of the linear force, see Eq. (44). This specific functional relationship between a and Σ_e follows from the requirement that, in the planar limit $\kappa \to 0$, our model must produce the same amplitude-stress relation as classical wrinkling theory [5]. More precisely, classical planar wrinkling theory predicts that the amplitude $\mathcal{A}_{el}$ of the wrinkling solution $u = \mathcal{A}_{el}\cos(kx)$, measured in units of the film thickness h, is equal to square of the excess film stress [9],

$$\mathcal{A}_{el} = \sqrt{\Sigma_e}. \tag{67}$$

This must be equal to the amplitude $\mathcal{A}$ of the solution $u = \mathcal{A}\cos(k_c x)$ of the standard SH equation (64), which is given by [14]

$$\mathcal{A} = \frac{2}{\sqrt{3}} u_* \sqrt{1 - A} \tag{68}$$

Equating the amplitudes yields

$$A = \frac{a}{a_c} = 1 - \frac{3\Sigma_e}{4u_*^2} \tag{69}$$

Finally, considering the definition of a in Eq. (44) in the planar case $\kappa = 0$ and inserting a_c from Eq. (54), we find

$$\tilde{a}_2 = -\frac{3\gamma_2}{4u_*^2}\left(\frac{3E_s}{E_f}\right)^{4/3} \tag{70}$$

We have thus determined all parameters of the effective theory with the exception of $\tilde{c}$, which enters through both c in Eq. (44) and u_* in (70), see Eq. (66). As shown in the next section, $\tilde{c}$ can be estimated by matching our model predictions with the experiments. Table I summarizes the results for our model parameters, retaining curvature terms up to $\mathcal{O}(\kappa^3)$, and is also reproduced in Table 1 of the Main Text.

Remark. In the above derivation, we have matched the amplitude-stress relationship using the plane-wave wrinkling solution. Alternatively, one can match the amplitude-stress relationship of wrinkling patterns using the hexagonal solution of the SH equation. The general procedure is identical to the one above. The hexagonal solution u_{H} of the standard SH equation is given by [14]

$$u_{\mathrm{H}} = \mathcal{A}\left[\cos(k_c x) + 2\cos\left(\frac{k_c x}{2}\right)\cos\left(\frac{\sqrt{3}k_c y}{2}\right)\right] \tag{71}$$

with

$$\mathcal{A} = \frac{2}{15}\left[Bu_* + \sqrt{(Bu_*)^2 + 15u_*^2(1 - A)}\right] \tag{72}$$

B vanishes in the planar case, where $\kappa = 0$. Classical planar wrinkling theory predicts the same solution, Eq. (71), with amplitude [9]

$$\mathcal{A}_{el} = \frac{2}{\sqrt{11 + 6\nu - 5\nu^2}}\sqrt{\Sigma_e} \tag{73}$$

Comparing the two amplitudes, we obtain

$$A = 1 - \frac{15\Sigma_e}{(11 + 6\nu - 5\nu^2)u_*^2} \tag{74}$$

from which a and $\tilde{a}_2$ follow again by Eqs. (44) and (54).

Hence, matching amplitudes in the hexagonal phase again leads to a linear relationship between A and Σ_e, but the prefactor differs compared with the plane-wave solution considered above.

However, irrespective of the chosen matching procedure, we obtain a linear relation between $\tilde{a}_2$ and $\tilde{c}$, leaving only one fitting parameter, $\tilde{c}$. Due to the linear dependence between $\tilde{a}_2$ and $\tilde{c}$ for both hexagonal and labyrinth patterns, one can use either matching relation to fit the experiments. Since the plane-wave (labyrinth) solution (67) leads to slightly simpler formulas, we choose the plane-wave matching in the following; that is, we assume that A and Σ_e are related by Eq. (69), and $\tilde{a}_2$ is given by Eq. (70). This convention means that we must determine $\tilde{c}$ by matching the theoretically predicted phase transition curve between the bistable and labyrinth states to the corresponding experimentally measured phase transition curve. The fitting value $\tilde{c}$ then automatically fixes the theoretical prediction for the second transition curve between hexagonal and bistable phase.

Phase diagram of the wrinkling morphology

The reduction of our effective theory to a standard Swift-Hohenberg equation allows us to make approximative predictions regarding the wrinkling morphologies. For the normal form, Eq. (65), three different wrinkling phases emerge depending on the choice of parameters A and B [14]:

$$\text{Unwrinkled:} \qquad 1 - A \leq 0 \tag{75a}$$

$$\text{Hexagons:} \qquad -\frac{1}{15}B^2 < 1 - A < \frac{4}{3}B^2 \tag{75b}$$

$$\text{Bistable phase:} \qquad \frac{4}{3}B^2 < 1 - A < \frac{16}{3}B^2 \tag{75c}$$

$$\text{Labyrinths:} \qquad \frac{16}{3}B^2 < 1 - A \tag{75d}$$

We recall that the coefficient B depends on κ via Γ_1, Γ_2, b and c, see Eq. (66), while A depends on the excess film stress and κ via Eq. (69). Substituting Eqs. (69) and (66) for A and B in Eq. (75), we obtain to leading order in κ the following stability criteria:

$$\text{Unwrinkled:} \qquad \Sigma_e \leq 0 \tag{76a}$$

$$\text{Hexagons:} \qquad -\frac{\rho}{20}\kappa^2 < \Sigma_e < \rho\kappa^2 \tag{76b}$$

$$\text{Bistable phase:} \qquad \rho\kappa^2 < \Sigma_e < 4\rho\kappa^2 \tag{76c}$$

$$\text{Labyrinths:} \qquad 4\rho\kappa^2 < \Sigma_e \tag{76d}$$

where

$$\rho = \frac{1}{\left[\eta^{1/3}(1-\nu)\tilde{c}\right]^2} \tag{76e}$$

The free parameter $\tilde{c}$ is a function of $\eta = 3E_s/E_f$ and ν. The functional form of $\tilde{c} = \tilde{c}(\eta, \nu)$ determines how the phase transition lines depend on those material properties. Comparison with our experimental data suggests, however, that the phase transition lines are in fact independent of η and ν (Fig. 3 of Main Text). In this case, ρ must be independent of η and ν, which means that

$$\tilde{c} = \frac{c_1}{(1-\nu)\eta^{1/3}}, \tag{77}$$

with fit parameter c_1. Adopting the ansatz (77), we find that $c_1 = 0.0188 \pm 0.0002$ gives the best fit to the experimental data (Fig. 3 of Main Text). The resulting good agreement with the data suggests strongly that the critical curves, which separate the different wrinkling phases in our experiments, are independent of material properties.

Hysteresis

We explain how the critical curves in Fig. 4 of Main Text are obtained. To this end, recall that the amplitude of the hexagonal solutions is given by Eq. (72). Inserting Eq. (69) for A gives

$$\mathcal{A} = \frac{2}{15}\left[Bu_* + \sqrt{(Bu_*)^2 + \frac{45\Sigma_e}{4}}\right] \tag{78}$$

To compare with the labyrinth solutions, we consider the measurable difference U_H of the maximal and minimal values of the hexagonal displacement field u_H (measured in units of h). Equation (71) implies that

$$U_\mathrm{H} = \max u_\mathrm{H} - \min u_\mathrm{H} = \frac{9}{2}\mathcal{A} \tag{79}$$

The prefactor in the last expression is due to the fact that u_H assumes its minimum at $-3\mathcal{A}$ and its maximum at $+3\mathcal{A}/2$.

To calculate the corresponding quantity U_L for the labyrinth solution u_L, we assume that labyrinths are locally described by the plane-wave $u_\mathrm{L} = \mathcal{A}\cos(k_c x)$. We then obtain with Eqs. (68) and (69)

$$U_\mathrm{L} = \max u_\mathrm{L} - \min u_\mathrm{L} = 2\sqrt{\Sigma_e} \tag{80}$$

Note that U_L is independent of curvature, whereas the square-root law for U_H is shifted horizontally and vertically by the Bu_*-terms (see Fig. 4b of Main Text). To first order in curvature, we have

$$Bu_* \simeq \frac{3\kappa}{4c_1} \tag{81}$$

DOI: 10.1038/NMAT4202

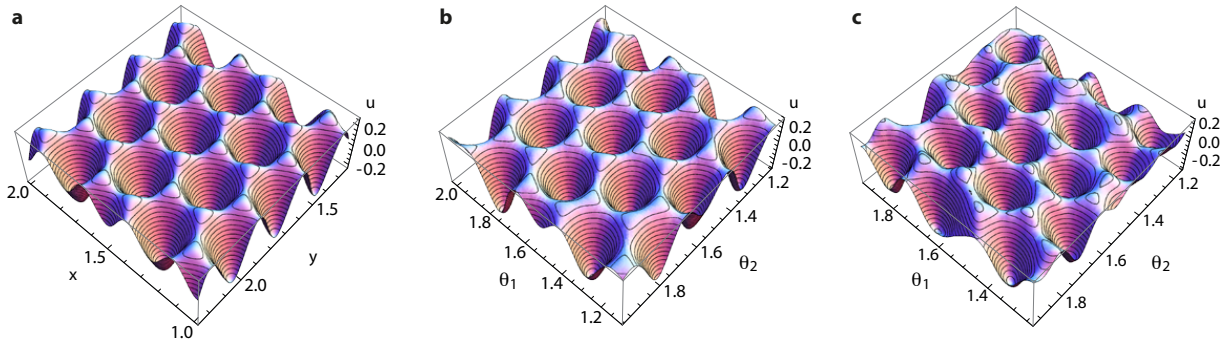

Fig. S1: Comparison of wrinkling morphologies in the hexagonal phase: (a) Planar analytical solution from Eq. (71), (b) numerical solution of the generalized Swift-Hohenberg theory from Eq. (43) (simulation parameters: $\gamma_0 = -0.08$, $a = 0.0151$, $c = 0.0095$, $R/h = 80$), and (c) 3D surface scan from experiments ($R = 20$mm, $h = 0.375$mm, $E_f = 2100$kPa, $E_s = 230$kPa). θ_1 and θ_2 denote polar angles.

yielding for the horizontal and vertical shifts (see Fig. 4b in the Main Text)

$$\delta\Sigma_e = \frac{\kappa^2}{20c_1^2}, \qquad \delta U_{\rm H} = \frac{9\kappa}{10c_1} \tag{82}$$

Based on the results for $U_{\rm L}$ and $U_{\rm H}$, we expect two hysteresis cycles (see Fig. 4 of Main Text). The first cycle is due to the shift $\delta\Sigma_e$, which creates a subcritical stability zone for the hexagonal solutions [14]. Increasing Σ_e from the unwrinkled phase, hexagons emerge at the onset $\Sigma_e = 0$. However, once they have formed, hexagons remain stable even if the excess stress Σ_e is subsequently reduced below the wrinkling onset $\Sigma_e = 0$. Only for $\Sigma_e < -\delta\Sigma_e$, hexagons loose stability and the unwrinkled solution remains as the only stable state. The second hysteresis cycle involves larger excess stresses (see Fig. 4a of Main Text). Starting from the hexagonal phase, hexagons remain stable if the excess stress is increased into the bistable phase [14]. Only if Σ_e is increased beyond the bistable-to-labyrinth transition line, hexagons loose their stability and the system jumps to a labyrinth state. Upon decreasing Σ_e from the labyrinth phase, the system adopts a different path as labyrinths remain stable throughout the bistable phase; a transition to hexagons happens when Σ_e is decreased below the critical value that separates the hexagonal from the bistable phase.

Validation of hexagonal patterns

To test our effective theory further, we compare the planar hexagon solution, Eq. (71), with the numerical solution of Eq. (43) on a spherical geometry (Fig. S1a,b). The good agreement between analytical and numerical solution confirms that the effective theory is indeed well approximated by the standard planar SH equation (65). These results corroborate that once hexagons are selected, curvature has negligible influence on their morphology. Moreover, analytical and numerical solutions compare well with the experimentally determined 3D surface scans (Fig. S1c), demonstrating that the presented effective theory is able to reproduce the morphological details of thin film buckling patterns.

TOROIDAL GEOMETRIES

We consider a torus with major radius R_1 and minor radius R_2 measured in units of h. Using Eq. (1) and the standard surface parametrization $\mathbf{S} = [(R_1 + R_2\cos\theta_2)\cos\theta_1, (R_1 + R_2\cos\theta_2)\sin\theta_1, R_2\sin\theta_2]$ with coordinates $(\theta_1, \theta_2) \in [0, 2\pi) \times [0, 2\pi)$ we obtain the metric tensor

$$(a_{\alpha\beta}) = \begin{pmatrix} (R_1 + R_2\cos\theta_2)^2 & 0 \\ 0 & R_2^2 \end{pmatrix} \tag{83}$$

Equation (5a) yields for the curvature tensor

$$(b_{\alpha\beta}) = \begin{pmatrix} -\cos\theta_2(R_1 + R_2\cos\theta_2) & 0 \\ 0 & -R_2 \end{pmatrix} \tag{84}$$

and, from Eq. (26), one finds mean and Gaussian curvature as

$$\mathcal{H} = -\frac{1}{2}\left(\frac{\cos\theta_2}{R_1 + R_2\cos\theta_2} + \frac{1}{R_2}\right) \tag{85a}$$

$$\mathcal{K} = \frac{\cos\theta_2}{R_1R_2 + R_2^2\cos\theta_2} \tag{85b}$$

Recall that the coefficients $\tilde{a}$, $\bar{\gamma}$, and $\tilde{a}_2$ were determined in the previous section using asymptotic comparison with the flat case. Hence, the expressions for these coefficients remain valid for toroidal geometries. Moreover, we observe that only the symmetry-breaking term in Eq. (34) contains contractions of the curvature tensor of first order, whereas the coefficients (33c) only depend on curvature at second or higher order. For instance, for

Fig. S 2: Wrinkling morphologies on a toroidal geometry with $R_1 = 80$ and $R_2 = 16$ for increasing excess film stress: (a) $\Sigma_e = 0.25$, (b) $\Sigma_e = 0.5$ and (c) $\Sigma_e = 2.0$. As in spherical geometries, one observes a transition from hexagonal to labyrinth-like patterns with increasing excess stress Σ_e. However, in contrast to the spherical case, the non-constant curvature on the torus can lead to local symmetry-breaking, i.e., at intermediate values of Σ_e labyrinth patterns are more likely to emerge at the inner saddle-like regions of the torus, see (b), whereas hexagons remain stable in the outer regions of the torus, where the two principal curvatures have the same sign resulting in a larger mean curvature. Simulation parameters are $\gamma_0 = -0.079$, $c = 0.075$, (a) $a = 0.017$, (b) $a = 0.016$, and (c) $a = 0.007$, using an unstructured surface triangulation with $> 26,000$ nodes.

a toroidal geometry with $R_1 = 80$, $R_2 = 16$, and $\eta = 0.33$ as shown in Fig. S2, we have $\gamma_0 = -0.079$, so that $|\gamma_0|$ is much larger than the maximum curvature correction $\max_{\theta_1,\theta_2} |\mathcal{R}/6| \approx 0.0007$. We can therefore neglect curvature corrections in the coefficients (33c).

Simulations of Eq. (34) confirm that a symmetry-breaking transition from hexagonal to labyrinth-like structures can also be observed on toroidal geometries when the excess stress is increased (Fig. S2). However, as curvature is now spatially varying, we find that the transition occurs first in the inner regions of the torus, where the principle curvatures have opposite sign (Fig. S2b). In the outside regions, where both principal components have the same sign, hexagons remain stable for relatively larger overstresses, until they become also unstable eventually (Fig. S2c).

In summary, Fig. S2 illustrates that the generalized theory derived above can be applied to arbitrarily curved surfaces.

[1] P. G. Ciarlet. *Mathematical elasticity, vol. III: Theory of shells*. North Holland, 2000.
[2] D. Breid and A. J. Crosby. Curvature-controlled wrinkle morphologies. *Soft Matter*, 9:3624–3630, 2013.
[3] M. M. Müller, M. Deserno, and J. Guven. Interface-mediated interactions between particles: A geometrical approach. *Phys. Rev. E*, 72(6):061407, 2005.
[4] W. Helfrich. Elastic properties of lipid bilayers: theory and possible experiments. *Z. Naturforsch.*, 28(11):693–703, 1973.
[5] Z. Y. Huang, W. Hong, and Z. Suo. Nonlinear analyses of wrinkles in a film bonded to a compliant substrate. *J. Mech. Phys. Solids*, 53:2101–2118, 2005.
[6] J. Swift and P. C. Hohenberg. Hydrodynamic fluctuations at the convective instability. *Phys. Rev. A*, 15(1):319–328, 1977.
[7] M. C. Cross and P. C. Hohenberg. Pattern formation outside of equilibrium. *Rev. Mod. Phys.*, 65(3):851–1112, 1993.
[8] H. G. Allen. *Analysis and Design of Structural Sandwich Panels*. Pergamon, New York, 1969.
[9] S. Cai, D. Breid, A. J. Crosby, Z. Suo, and J. W. Hutchinson. Periodic patterns and energy states of buckled films on compliant substrates. *J. Mech. Phys. Solids*, 59:1094–1114, 2011.
[10] L. D. Landau and E. M. Lifshitz. *Elasticity theory*. Pergamon Press, New York, 1975.
[11] Y. Jeong, Y.-C. Chen, M. K. Turksoy, S. Rana, G. Y. Tonga, B. Creran, A. Sanyal, A. J. Crosby, and V. M. Rotello. Tunable elastic modulus of nanoparticle monolayer films by host–guest chemistry. *Advanced Materials*, in press, doi: 10.1002/adma.201401226, 2014.
[12] G. Cao, X. Chen, C. Li, A. Ji, and Z. Cao. Self-assembled triangular and labyrinth buckling patterns of thin films on spherical substrates. *Phys. Rev. Lett.*, 100(3):036102, 2008.
[13] J. Yin, Z. Cao, C. Li, I. Sheinman, and X. Chen. Stress-driven buckling patterns in spheroidal core/shell structures. *Proc. Natl Acad. Sci.*, 105(49):19132–19135, 2008.
[14] A. A. Golovin and A. A. Nepomnyashchy. *Self-assembly, pattern formation and growth phenomena in nano-systems*. Springer, Dordrecht, 2006.